State selective electron capture at low energies

Bliek, Frederik Willem

7 ATOMIC DATA FOR CHARGE EXCHANGE SPECTROSCOPY

Introduction

The bulk plasma in a fusion reactor is confined by a set of closed magnetic surfaces (see figure 1) and the particles primarily flow along these surfaces. Although the transverse diffusion is much higher than expected from neoclassical models the anomalous transport is small compared to the parallel flow. In the outside Scrape Off Layer (SOL) particles flow along magnetic field lines to the point where these magnetic field lines are in contact with the surface of the vessel. The flux, speed, masses and incident angle on the surface determine the sputtering and release of elements like C, Be and Ni into the plasma. These ions are generally qualified as 'plasma impurities' since they have many undesirable effects. In tokamak plasmas already very small amounts of highly charged impurity ions lead to an enormous increase in the radiation and particle losses, a decrease in Ohmic heating and they can be the origin of various plasma instabilities.

The way to control these impurities is found by creating a poloidal magnetic null or X-point within the plasma volume (see figure 1). The outer magnetic field line in not closed any more and its strike zones on the divertor target plates are the only direct plasma-surface contacts. Neutrals that enter the plasma are ionized and captured by this outer magnetic field line and fed into the divertor before they can penetrate the bulk plasma. The design of pumped divertors seeks to maximize the particle flow into the divertor where they can be pumped away from the bulk plasma. Further with high densities in the SOL a strong radiating plasma of low temperature ($T_e \approx 1 - 100\ eV$) and high density ($n_e \geq 10^{14} cm^{-3}$) may be obtained, minimizing the sputtering. These high density plasmas in the SOL can be obtained by means of heavy gas puffing.

Present divertor studies at JET concentrate on the choice of target plate materials and the puffing gas species to control the introduction and transport of impurities and their effect on more general plasma conditions like the diffusion coefficients. Several diagnostics like Langmuir Taylor probes, Charge eXchange Spectroscopy (CXS), bolometers, fast CCD-cameras, soft X-ray cameras etc. are available to probe the physical processes in the SOL and divertor regime. Among these diagnostics CXS is the one which in principle can determine the local (impurity) ion densities and temperatures provided that accurate atomic cross section data are available for the CX-process and the competing electron impact

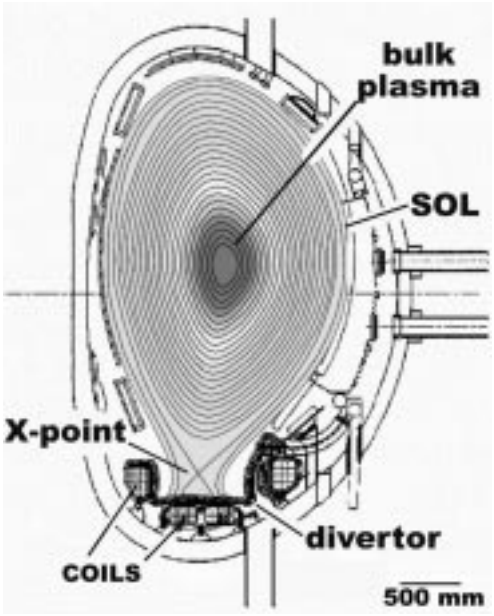

Figure 1 The JET pumped divertor (mark I configuration).

excitation process. The neutral deuterium heating-beam based CXS diagnostic has shown that these plasma quantities can be determined with an accuracy in the order of 20%.

This chapter will concentrate on the cross section data that are required for CXS-diagnostics based on neutral helium heating beams and the role of metastables present in these beams. In the last part of this chapter the significance of the low energy cross section data for CXS observations of the SOL and divertor will be discussed in relation to the experiments that are described in this thesis. Furthermore it has to be noted that detailed spectroscopic observations of photon emission from interstellar nebulae and astrophysical plasmas allow for using similar techniques to diagnose the ionic properties of such plasmas. One of the most abundant species in these plasmas is hydrogen and in smaller concentrations light elements like carbon, nitrogen and oxygen. The temperatures are in the same order of magnitude as in the SOL of a tokamak and therefore similar cross section data are required for the diagnostics of such interstellar objects [124], [125], [96].

Charge eXchange Spectroscopy

In a plasma partially stripped ions in excited states are created via several collision processes like electron impact excitation and charge exchange. Provided that these collisional processes can be separated to an appropriate degree the latter process can be used as the driving reaction for CXS, which can be characerized by:

$$
\begin{aligned}
A^{q+}_{plasma} + B &\rightarrow A^{(q-1)+}_{plasma}(n\ell) + B^{+} \\
&\rightarrow A^{(q-1)+}_{plasma}(n'\ell') + B^{+} + h\nu
\end{aligned}
\tag{7.1}
$$

The emitted radiation $h\nu$ carries information about the plasma ion $A^{(q-1)+}_{plasma}$. The line intensity $I(\lambda)$ of the photon emission at wavelength λ is given by:

$$
I(\lambda) = \iint \delta(v_\lambda - v_{ion}\cos\alpha) k(v_{col}) n_{nb} f(v_{ion}) G d\Omega dv_{ion} \tag{7.2}
$$

with $\delta(v_\lambda - v_{ion}\cos\alpha)$ the Doppler shift due to the velocity v_{ion} of the ions with respect to the line of sight of the detector, n_{nb} the neutral beam density, $f(v_{ion})$ the velocity distribution of the ions, G a geometry factor, $d\Omega$ the observation solid angle and $k(v_{col})$ the rate coefficient. The fact that the rate coefficient for the emission of photons, which is given by:

$$
k(v_{col}) = v_{col} \cdot \sigma(v_{col}) \tag{7.3}
$$

depends on the cross section σ implies that accurate cross section data are necessary to reveal the plasma parameters. In this formula v_{col} represents the relative velocity between the collision partners.

The local impurity ion temperature T_i can be deduced from the spectral line by using:

$$
T_i = \frac{m_i}{k_B} \left(\frac{c\lambda_w}{\lambda_0 \sqrt{8 \ln 2}} \right)^2 \tag{7.4}
$$

where m_i is the impurity mass, k_B the Boltzman constant, c the speed of light, λ_w the full width at half maximum of the line and λ_0 the wavelength of the transition. From the wavelength difference, $\Delta\lambda_{rot}$, between the observed CX-line and the unperturbed line the plasma rotation velocity, v_{rot}, can be deduced:

$$
v_{rot} = c\frac{\Delta\lambda_{rot}}{\lambda_0} \tag{7.5}
$$

The measured photon flux per square meter, ϕ, of the emitted photons is proportional to the local impurity density, n_{imp}, and the local neutral beam density, n_b, in the plasma:

$$
\phi = \frac{1}{4\pi} \int k(v_{col})\ n_b\ n_{imp} \cdot dl \tag{7.6}
$$

where the integral is taken along the line of sight.

The neutral acting as an electron donor in reaction 7.1 is either supplied by a neutral beam injected into the plasma with a specific energy and in this case one speaks of active CXS, or one can observe the CX-signal resulting from collisions between ions and neutrals inherently present in the plasma. In the latter case one speaks of passive CXS.

One other very important process in neutral beam based charge exchange spectroscopy is beam excitation:

$$\begin{Bmatrix} A^{q+}_{plasma} \\ e^- \end{Bmatrix} + B_{beam} \rightarrow \begin{Bmatrix} A^{q+}_{plasma} \\ e^- \end{Bmatrix} + B_{beam}(n\ell) \rightarrow \begin{Bmatrix} A^{q+}_{plasma} \\ e^- \end{Bmatrix} + B_{beam}(n'\ell') + h\nu \quad (7.7)$$

This process can directly be used for Beam Emission Spectroscopy (BES). later it will be discussed that process 7.7 is of relevance for CXS. The excitation can lead to the creation of neutrals in long lived metastable states. Since high n-states in impurity ions can directly be populated by electron capture from such metastables CXS observations can become severely influenced by the presence of metastables in the neutral beams as described in paragraph 7.

Neutral Beam based CXS

The primary interest in neutral beam based CXS is that it offers a possibility to observe the normally non-radiating fully stripped ions in the plasma-core by inducing emission. One of the major interests in current fusion plasma research is the understanding of the production, transport and slowing down of the α-particles resulting from the ^{2}D + ^{3}T fusion reaction. The removal of α-particles is of major interest for the next-step device in fusion research: ITER, since the accumulation of He-ash can limit the performance. The problem is that the α-particles produced in the D-T reaction should be contained long enough in the plasma to transfer their energy to the plasma to keep the fusion reaction going, but it should be removed to prevent an accumulation of He-ash which can suffocate the DT-reaction. A tool to observe the fusion born He is the HeII($n = 4 \rightarrow n = 3$) line emission resulting from charge-transferring collisions between He^{2+} ions and neutral beam particles (see figure 2). Such neutral He heating beams are regularly used for diagnostic purposes at several tokamaks like: TEXTOR (Jülich, Germany), JET (Abingdon, UK) and JT60 (Naka, Japan). These diagnostics require absolute state selective cross section data for He^{2+} + He collisions for an accurate determination of the He density and temperature. The experimental results that are obtained for this collision system by means of PES will be reviewed and discussed. In the following section the implications for CXS diagnostics will be discussed. Especially the role of a small fraction of metastables present in the neutral He-beams will be treated and extended to a more general issue in neutral beam based CXS.

The geometric configuration of the JET CXS facilities has been reported in several papers [126], [127] and will only shortly be discussed in this paragraph. The active CXS diagnostics elements are constructed around the neutral heating beams of JET. ^{1}H, ^{2}D, ^{3}T and ^{3}He or ^{4}He can be fired into the plasma at energies ranging from 80 to 150 keV. The neutral beams have an area of approximately 300 cm^2 in the plasma center and the optical viewing aperture is ~ 5 cm^2. The radiative lifetime of different l-states of the $n = 4$ shell are in the range of 0.77 to 14.2 ns. This implies that the decay length along the beam line, for a plasma temperature of 20 keV is in the order of 2 mm. Therefore the radiation is localized and reflects the reactions in the observed volume. Discrimination from background and simultaneous measurement of the plasma edge properties is possible by modulation of the neutral beam or by pre- and post beam measurements.

The photon emission resulting from reaction 7.1 due to the collisions between the neutrals B_{beam} and the (impurity) ions A^{q+}_{plasma} is observed with a multichord system consisting of 12 quartz fibres. The photons detected are analyzed by Czerny-Turner type spectrometers.

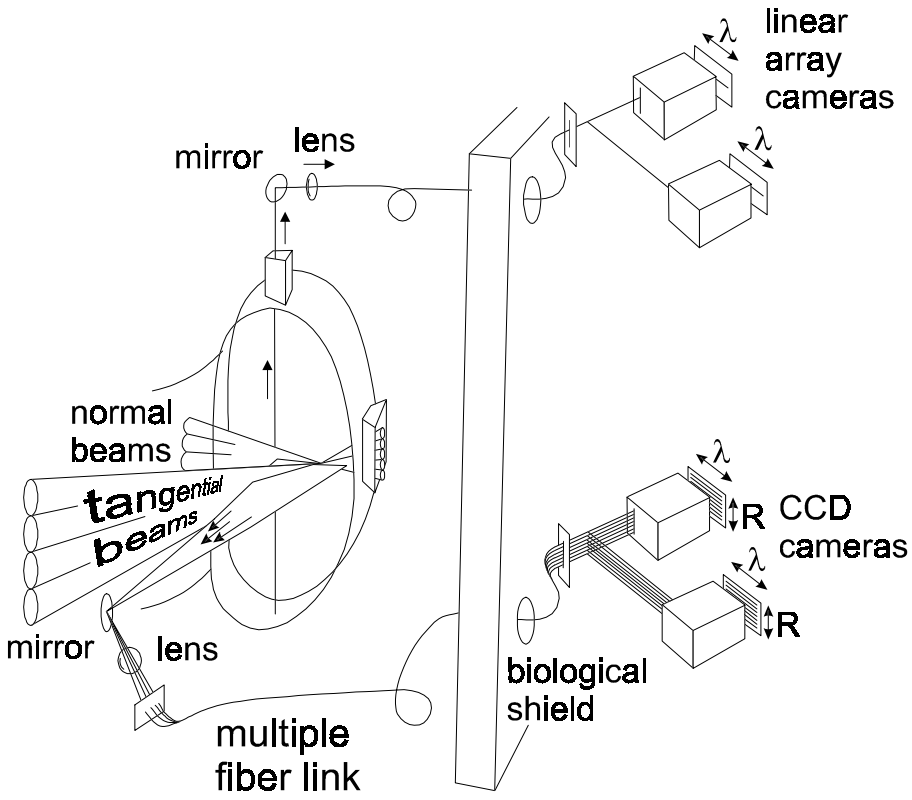

Figure 2 Artistic impression of the neutral beam based charge exchange spectroscopy diagnostics at JET.

For full CXS modelling accurate state selective cross section data are essential because the plasma conditions in large tokamaks are such that the $He^{+}(4\ell)$ states are fully redistributed to a nearly statistical population due to collisional mixing and the strong electric fields that are present in the plasma [128]. This implies that the population of the ℓ-states gives rise to different photon yields in a tokamak and in a field-free laboratory environment. Therefore state selective cross sections are necessary to predict the correct photon yield for the HeII($n = 4 \rightarrow n = 3$) line emission. Moreover the cross sections for a wide range of collision energies are needed. This paragraph gives a short description of the experimental investigation of charge exchange reactions in He^{2+} collisions with He in the energy range between 1 and 75 keV/amu. A more detailed description of these exepriments can be found in [129].

The interest in this collision system is not only due to possible applications but there is also a considerable fundamental interest because of the intrinsic symmetry of the system. The system can be regarded as the 'simplest' two-electron system in which one-electron capture can be studied, however the symmetry of this system together with the large exo- and endothermicity of the different one-electron capture channels severely complicates the theoretical description of the charge transfer process [86]. Shah et al. [130] investigated two-electron capture into the ground state of the projectile, which is a resonant process and exceeds one-electron capture at energies below 10 keV/amu. We will show that for collision energies below $\sim$ 10 keV/amu $He^{+}(n)$ can be produced via 2 different processes:

1. One-electron capture:

$$ {}_{p}He^{2+} +_{t} He(1s^2) \rightarrow_{p} He^{+}(n) +_{t} He(1s) \tag{7.8} $$

   and

2. capture into the ground state and simultaneous excitation of the target-ion:

$$ {}_{p}He^{2+} +_{t} He(1s^2) \rightarrow_{p} He^{+}(1s) +_{t} He^{+}(n) \tag{7.9} $$

   For completeness it should be mentioned that above $\sim$ 100 keV/amu excited target ions are produced via:

3. single ionization and simultaneous excitation of the target-ion:

$$ {}_{p}He^{2+} +_{t} He(1s^2) \rightarrow_{p} He^{2+} +_{t} He^{+}(n) + e^{-} \tag{7.10} $$

The subscripts p and t have been added to distinguish between the projectile and target respectively. Processes 7.8 and 7.9 are subject of our experimental investigation.

In a set-up for photon emission spectroscopy similar to the one described in chapter 3, only without the octpole, the HeII($np \rightarrow 1s$) Lyman transitions with $n = 2, 3$ and 4 at wavelengths of 30.4, 25.6 and 24.0 nm are measured with the grazing incidence VUV monochromator. The position sensitive detector of this monochromator allows for a simultaneous observation of all the HeII Lyman lines. The HeII($n = 4 \rightarrow n = 3$) line emission at 468.6 nm is observed perpendicular to the ion beam with the visible light spectrometer. This spectrometer is equipped with an imaging system that allows to scan the emission profile along the beam axis. This is an essential feature for the deconvolution of the emission profile into the contributions from the $He^+(4\ell)$ states (see Chapter 3). Here the four $He^+(4\ell)$ projectile states and the target excitation contribution have to be deconvoluted from the emission profile.

It should be noted that the contribution of the $4p$ state to the HeII($n =$

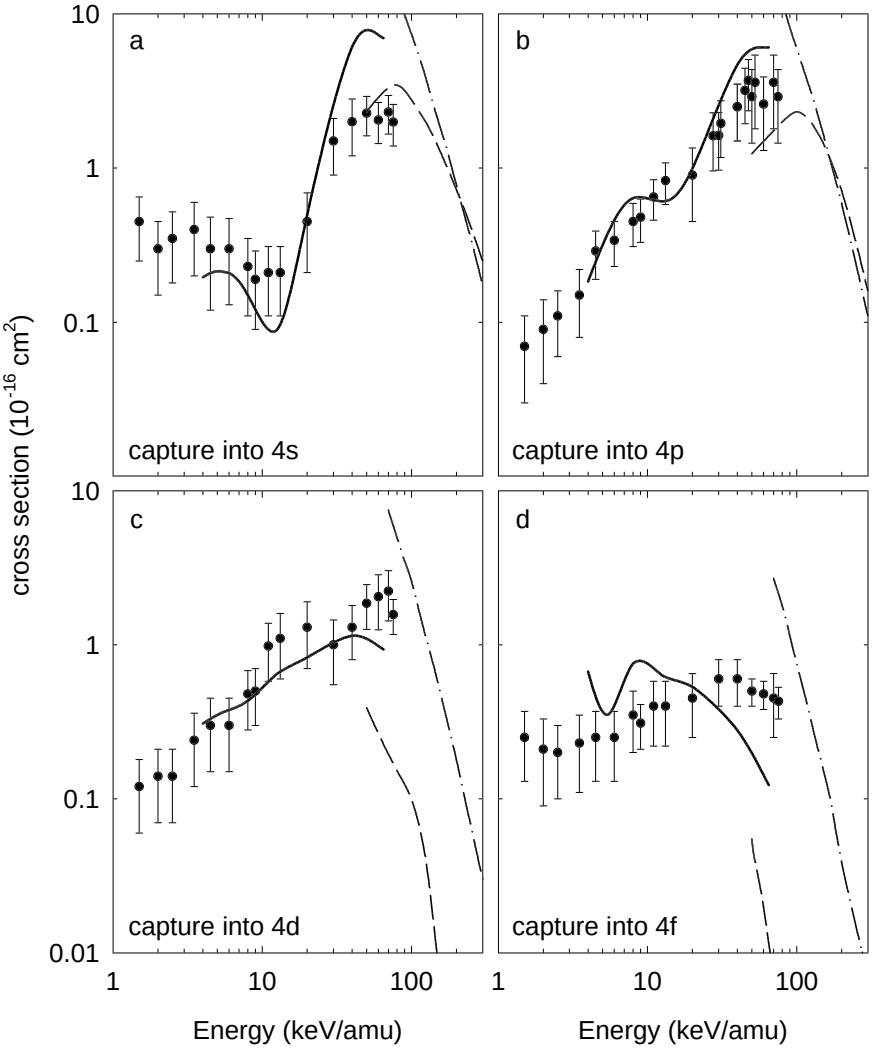

Figure 3 State selective He+(4ℓ) electron capture cross sections. a) $4s$, b) $4p$, c) $4d$ and d) $4f$. The circles mark the present experimental results. Only relative errors are shown. Theoretical curves: Fritsch AO (—) [86]; Olson CTMC [129] (- - -); Gayet CDWA [131] ($- \cdot -$).

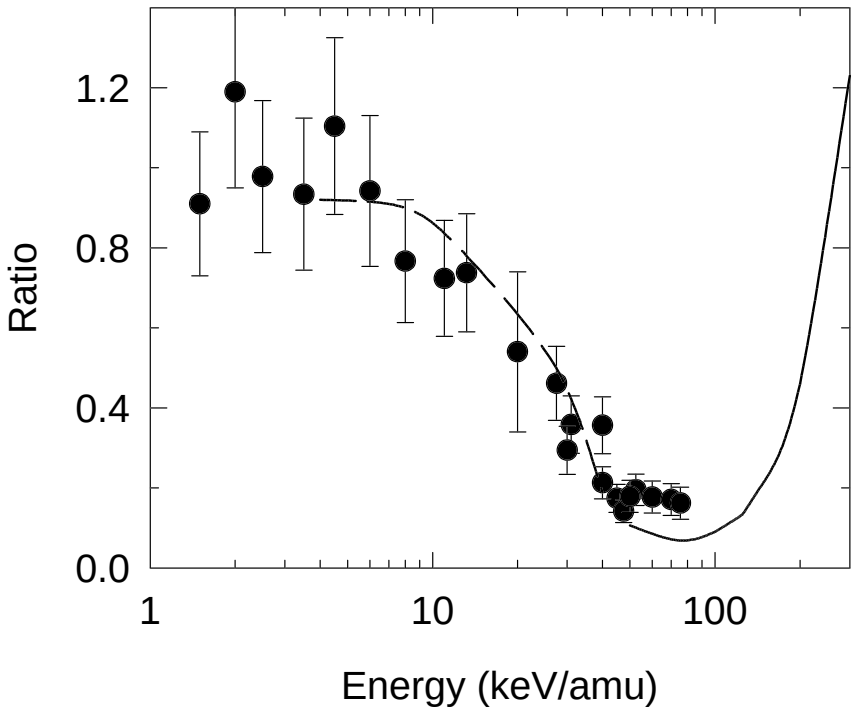

Figure 4 Ratio of simultanous electron removal and target-ion excitation cross sections and one electron capture cross sections as function of the collision energy. Experiment and CTMC calculation (—) are for HeII($n = 4 \rightarrow n = 3$) line emission. The broken curve denotes the results of the AO calculation for the ratio of HeII($n = 3$) production.

$4 \rightarrow n = 3$) emission line is very small due to the small branching ratio of only 4%. However the $4p$ population can be determined accurately from the HeII($4p \rightarrow 1s$) transition in the VUV. In this way the number of fit parameters is reduced from 5 to 4. Furthermore it should be noted that the magnitudes obtained for the individual $He^+(4\ell)$ one-electron capture contributions are sensitive to the exact shape of the emission profile, although their sum is nearly insensitive. Therefore the contributions of one-electron capture and simultaneous electron removal on the one hand and the contribution of target excitation on the other hand can be determined accurately.

In the following part the experimental results will be compared with various theoretical predictions with two aims in mind:

- check the validity of the various theoretical models.
- derive a set of "recommmended" cross sections to be implemented in the Atomic Data and Analysis Structure (ADAS).

The experimental results are shown in figure 3, 5 and 4. together with corresponding theoretical predictions. From figure 4 it can be seen that below 10 keV/amu one-electron capture (process 7.8) and target excitation (processes 7.9 and 7.10) are equally likely, which is due to of the symmetry of the collision system [132], [86]. With increasing energies one-electron

capture becomes more and more important and exceeds the target excitation channel by a factor of 6 at 50 keV/amu. According to the CTMC calculations the probability for one-electron capture decreases again and eventually even drops below that for target excitation at energies above 250 keV/amu.

Figure 5 depicts the state selective one-electron capture cross sections as derived from the fits of the emission profiles together with the various theoretical results that are available. Among them there are the Continuum Distorted Wave Approximation (CDWA) calculations of Gayet et al. [131]. From comparison of experimental data with previous CDWA calculations for collisions on atomic hydrogen it is assumed that these calculations are reliable at energies above 150 keV/amu. For this collision system the CDWA calculations clearly overestimate the cross sections below 150 keV/amu. The AO calculations are generally very close to the experimentally determined cross sections. The structures found in the capture probabilities by the AO method can however not be confirmed by the experimental data. At the highest energies the $4s$ state is overestimated by a factor ~ 4. The CTMC calculations connect the experimental results for the $4s$ and $4p$ state very well with the CDWA above 150 keV/amu.

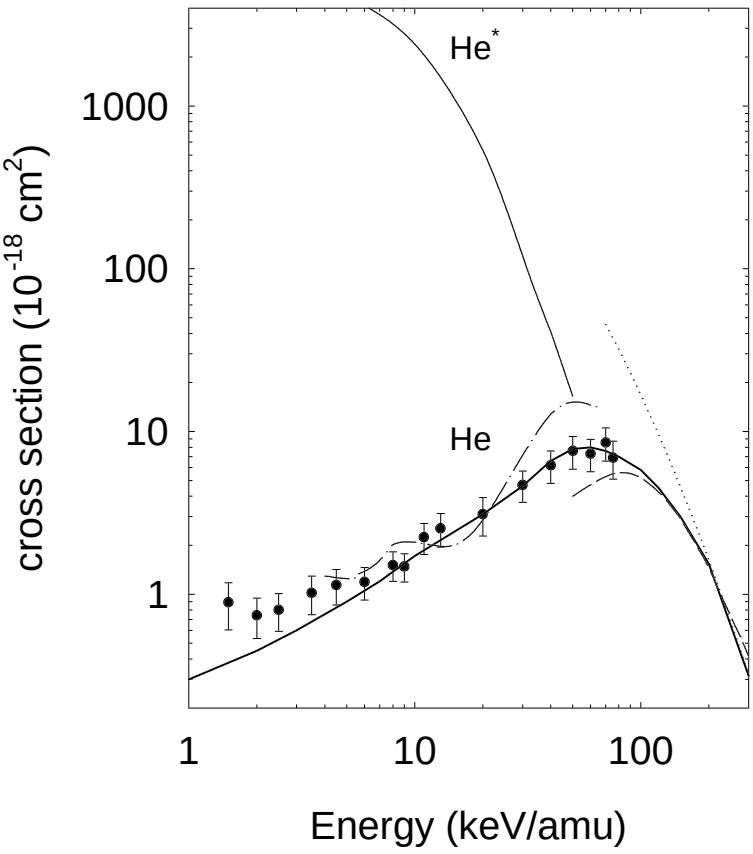

Figure 5 Total electron capture cross section into the $n = 4$ shell by He^{2+} ions colliding on He. (•) Experimental Data; $(- \cdot -)$ AO Fritsch; $(- - -)$ CTMC Olson; $(\cdots)$ CDWA Gayet; (—) CTMC for capture from He($2\ ^1S, 2\ ^3S$).

However the CTMC calculations clearly underestimate capture into the $4d$ and $4f$ state.

The minimum that is observed in the $4s$ state around 10 keV/amu seems to be confirmed by the AO calculations but this minimum is most likely an artefact of our deconvolution method of the emission profiles. Since the lifetime of the $5g$ state is comparable to that of the $4s$ state the depopulation of the $5g$ state via the $5g \rightarrow 4f \rightarrow 3d$ cascade is in the deconvolution ascribed and added to the $4s$ state. Below 8 keV/amu the capture into the $5g$ state becomes significant. From the ratio of the HeII($3p \rightarrow 1s$) and the HeII($4p \rightarrow 1s$) line emission we find a power α of approximately 5 for a $\frac{n}{(n+1)^\alpha}$ scaling that connects the different n-shells. Using this α-scaling to calculate capture into the $n = 5$ shell and assuming a statistical population of the ℓ-states for the lowest collision energies one can estimate the contribution of the cascade from the $5g$ state. This leads to a consistent picture with the observed cross sections and it is found that the contribution of the $5g$ state exceeds the actual contribution of the $4s$ state below 5 keV/amu by a factor of 3 to 5.

Figure 5 depicts the total charge transfer cross section to the $n = 4$ shell together with the theoretical predictions and the recommended cross section for the ADAS database. Because of the $5g$ cascade correction as mentioned above, the recommended curve is lower than the experimental data below 10 keV/amu. From 10 keV/amu up to the maximum of the experimental cross section the recommended curve follows the experimental data and above these energies up to 200 keV/amu the CTMC calculations. Above 200 keV/amu the CDWA calculations are used.

The role of metastables in neutral beam based CXS

At the JT-60 tokamak in Japan 90 keV neutral He beams have been used for heating the plasma. Recent experiments seem to indicate that 20% of the beam is in the He($1s2s$) metastable state [133]. These metastables are very easily ionized via ion and electron impact when entering the plasma. This would imply that 20% of the injected power is deposited very close to the walls and the resulting heating effect could cause severe damage. At JET the fraction of metastables in the He beams is much smaller and is estimated to be at most 7% [25]. Despite the fact that the largest fraction of atoms in the He$(1s2s)^3S$ state are ionized while entering the plasma, signals related to excited states are observed along the whole penetration path of the beams [25]. This indicates that ground state He-atoms of the injected beam are excited by the interaction with the plasma. There is a dynamical balance between excited and ground state populations.

Since the high-n states of hydrogen-like atoms can almost resonantly be populated by electron capture from metastable helium atoms the question arises whether the CXS signals, which originate from decay of these high-n states, may be influenced by a small fraction of metastable ions in the heating beams. Answering this question is hampered by two facts:

- The metastable fraction of the neutral heating beam is not (accu-

rately) known and there are no methods available yet to measure this fraction. This issue will be discussed in the next paragraph.

- Experimentally direct measurements of cross sections for capture from metastable states are impossible since there are no metastable He gas targets available with sufficient densities to perform PES experiments.

Therefore one has to rely on the calculations.

The effect of metastables on the He^{2+} diagnostics

For the He^{2+} + He^* system calculations have been performed by Olson [129] and Fritsch [86] and the results are summarized in figure (5).

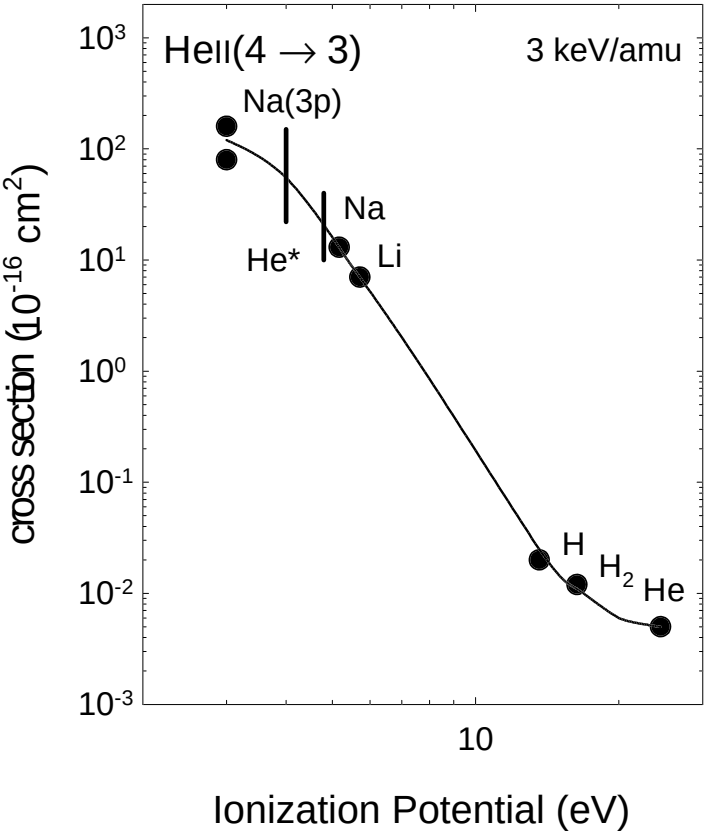

Figure 6 Summary of the HeII($n = 4 \rightarrow n = 3$) line emission cross sections resulting from He^{2+} ions colliding on helium [129], atomic [79] and molecular hydrogen [67], lithium [82] and ground state [134] and excited sodium [135]. The two entries for laser excited sodium indicate the resukts for the cases that the Na($3p$) dumbbell is aligned parallel and perpendicular with respect to the beam axis. The positions of the He(2^1S) and the He(2^3S) atoms having ionization potentials of 4 and 4.8 eV respectively are represented by the vertical bars.

From this figure it can be seen that at the lowest energies capture from metastable He state has a cross section that is a factor of 10^4 larger than the one for ground state He. The situation at the energies of the JET beams (40 keV/amu) is less dramatic and the cross sections differ only by a factor of five. Before looking into more detail what the consequences of the difference in capture probability are we will first check the validity of the predictions by the CTMC calculation.

The effect of the binding energy of different targets has been investigated systematically. The cross sections for electron capture by He^{2+} ions from several targets have been measured at a collision energy of 3 keV/amu to see the dependence of the cross section on the ionization energy and they are depicted in figure 6. The figure suggest that the cross section is monotonically dependent on the ionization potential of the target. Therefore the result for metastable He can be found by interpolating between the result for Li, Na and laser excited Na($3p$). It should be noted that there are two entrees for laser excited Na($3p$). Depending on the

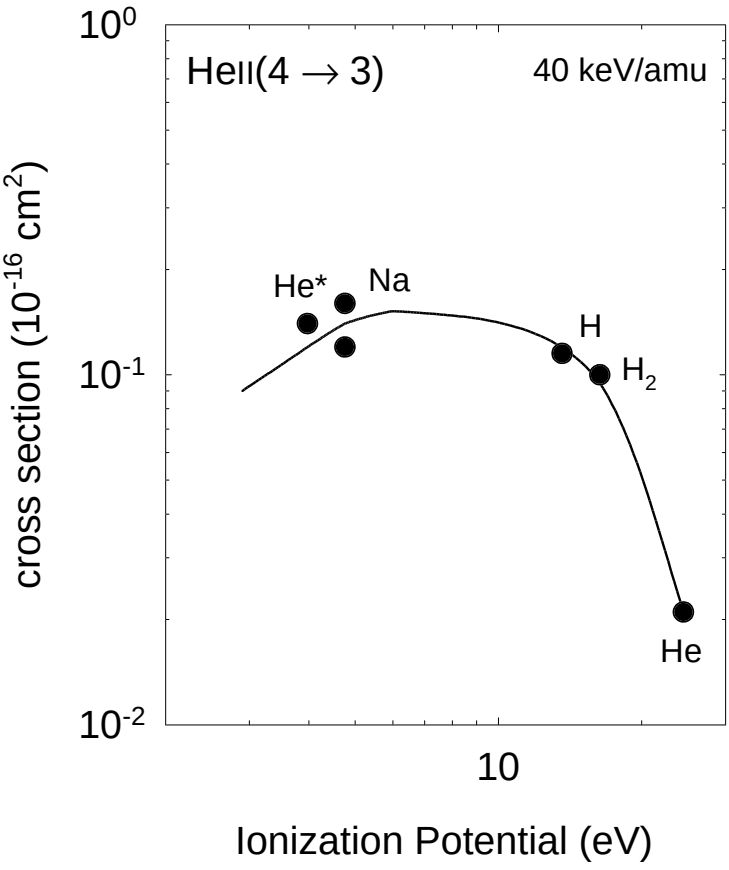

Figure 7 Summary of the HeII($n = 4 \rightarrow n = 3$) line emission cross sections resulting from He^{2+} ions colliding on helium [129], atomic [79] and molecular hydrogen [67], lithium [82] and ground state [134] and excited sodium [135]. The two entries for laser excited sodium indicate the resukts for the cases that the Na($3p$) dumbbell is aligned parallel and perpendicular with respect to the beam axis. The positions of the He(2^1S) and the He(2^3S) atoms having ionization potentials of 4 and 4.8 eV respectively are represented by the vertical bars.

alignment of the Na($3p$) orbital with respect to the ion beam axis the cross sections differ by a factor of two, whereby the aligment perpendicular to the beam axis yields the largest cross section.

To check whether these predictions also hold at heating beam energies a compilation of HeII($n = 4 \rightarrow n = 3$) emission cross section is shown in figure 6. The results for laser excited Na($3p$) are not shown since the energy range for these measurements is limited to 10 keV/amu. So the results for ground state Na should serve as a guideline for the metastable He comparison. At higher energies the results for ground state Na are extrapolated using the Bohr-Lindhard scaling as described in chapter 2.

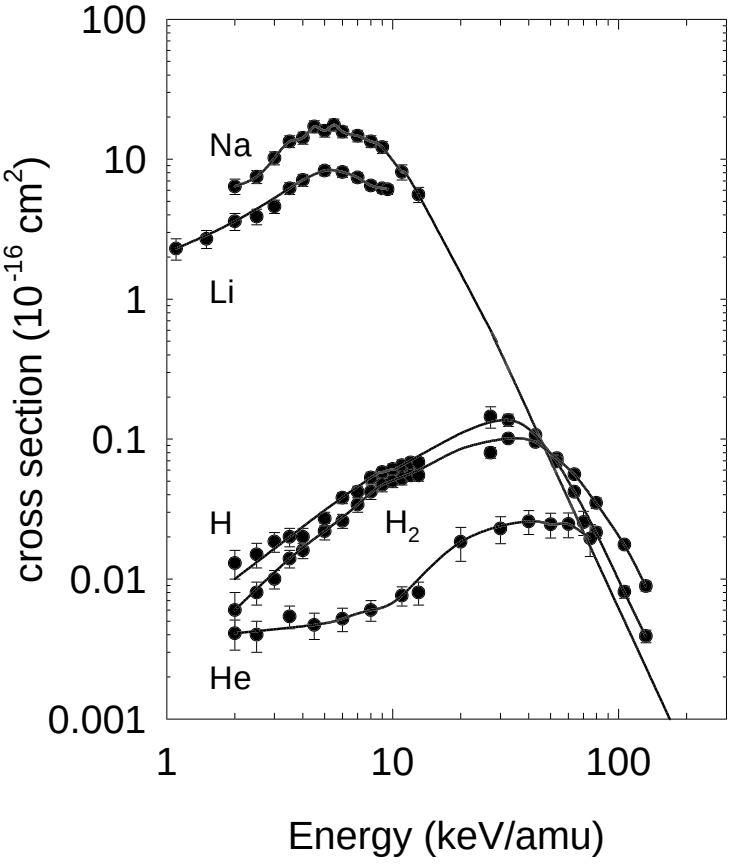

Figure 8 Full collection of HeII($n = 4 \rightarrow n = 3$) emission cross sections following electron capture from different targets, A, by He^{2+} ions.

Returning to the CTMC results it is clear that the one-electron capture probability by He^{2+} from He(2^1S, 2^3S) is much higher than the probability for capture from He($1s^2$). This would lead to significant increase of the observed CXS signals even for only a small fraction of the neutral beams in a metastable state. However around the helium heating beam energies of JET the ratio between these two cross sections strongly depends on energy. This has some important consequences for the derived ion density because the collision energy enters equation 7.2 via the rate coefficient (eq. 7.3). Although the average collision energy does not depend on the plasma temperature, the distribution of collision velocity becomes larger with increasing plasma temperatures. Therefore also collisions with a much smaller energy in the center of mass frame start to contribute to

the line emission where the cross section for capture from metastable hydorgen is much higher. The consequence is that the thermally averaged rate coefficient, g:

$$g = \int_{-\infty}^{\infty} k(|\overrightarrow{v}_b - \overrightarrow{v}_p|)\ f(\overrightarrow{v}_p)\ d\overrightarrow{v}_p, \tag{7.11}$$

for a fixed neutral beam energy, depends on the plasma temperature. In this equation v_b and v_p are the velocity of the beam and plasma particles respectively, $k(v_{col})$ the rate coefficient at the collision velocity, v_{col}, and $f(v_p)$ the velocity distribution of the plasma particles. As a consequence the plasma ion density that is derived from the CXS signals has to be corrected as a function of the plasma temperature.

If a fraction p of the neutral beam is in a metastable state the increase of the CXS signal, γ, can be calculated as follows:

$$\gamma = p(\frac{g_m}{g_{gr}} - 1) \tag{7.12}$$

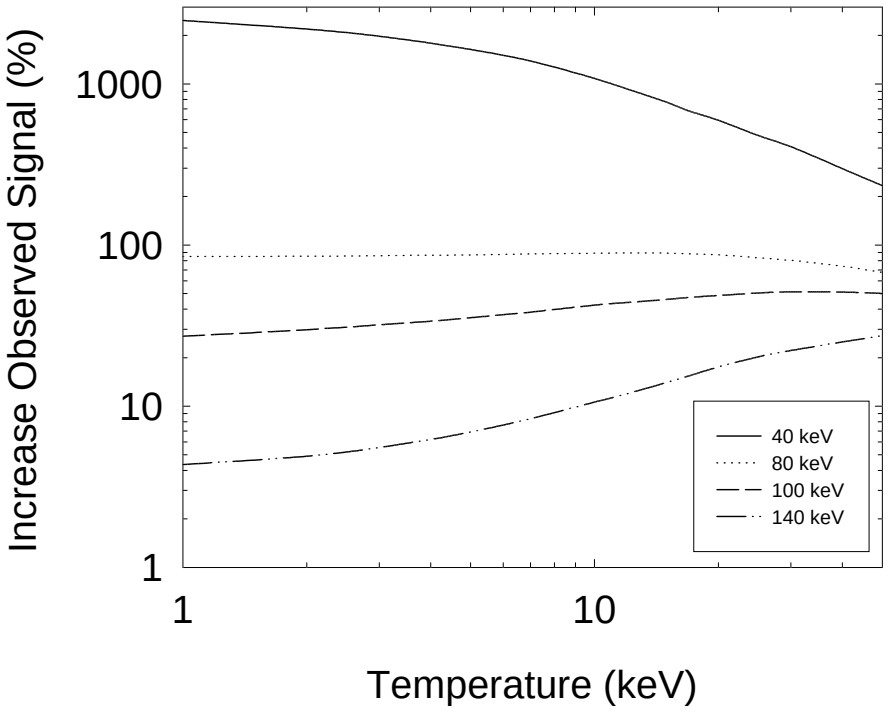

Figure 9 Increase of the CXS signal as a function of the average plasma temperature when a fraction of 2% of metastables is present in the neutral beams.

with g_{gr} and g_m the thermally average rate coefficients for capture from ground state and metastable state helium respectively. Figure 9 shows a plot of γ (in %) as a function of the plasma temperature for several neutral beam energies, where a fraction of 2% of the neutral beam is assumed to be in a metastable state. The situation for the helium beams of JET with typical energies in the range between 80 and 150 keV is already dramatic. Although for a beam energy of 80 keV the correction for the density does not depend so strong on energy, the He^{2+} density will be overestimated

by almost 90%. The situation at TEXTOR is even worse: here a fraction of 2% metastables would already increase the signals at the cold plasma edge by a factor of approximately 25. At the hot central plasma core the situation is a little better but still the signal resulting from capture from the ground state will already be blended by capture from metastable states if only a small amount of metastables is present.

Furthermore it should be noted that since this correction depends on the plasma temperature and typically the temperature in a tokamak varies as a function of the radial position [136]:

$$T_i = T_{i0}\left(1 + q_a \frac{r^2}{a^2}\right)^{-\frac{4}{3}} \tag{7.13}$$

where Ti and T_{i0} are the ion temperature at radial position r and the central ion temperature respectively and a is the minor radius. It is clear that the correction factor γ varies with the position along the neutral beam.a density correction has to be used that depends on the position of the origin from where the photons are emitted. In case that neutral beams with an energy of 140 keV are used the He^{2+} density in the plasma core will be overestimated more than the density at the cold plasma edge for 40 keV neutral He beams the situation is reversed.

The effect on the C^{6+} diagnostics

In order to check the situation for the detection of the main plasma impurity carbon a similar cross check as for the He^{2+} + He case as described in the previous section has been made for C^{6+} + He at 4 and 40 keV/amu [137], [138]. Figures 10 and 11 depict the CVI($n = 7 \rightarrow n = 6$) line emission cross section as a function of the ionization energy of the target. Also here the cross sections for electron capture by C^{6+} ions from metastable ions can be estimated. At 4 keV/amu the cross section for capture from metastable He is estimated to be approximately 5 orders of magnitude higher than that for capture from ground state He. At 40 keV/amu the difference is less, but still the difference is approximately 3 orders of magnitude. This implies that in practice CXS-signals from ground state He can be completely masked by photon emission resulting from capture from metastable Helium.

The overwhelming influence of the minor He($2^1S,\ 2^3S$) component of the neutral beam on the CVI($n = 7 \rightarrow n = 6$) emission can possibly be used to determine for the first time the metastable fraction in the beam.

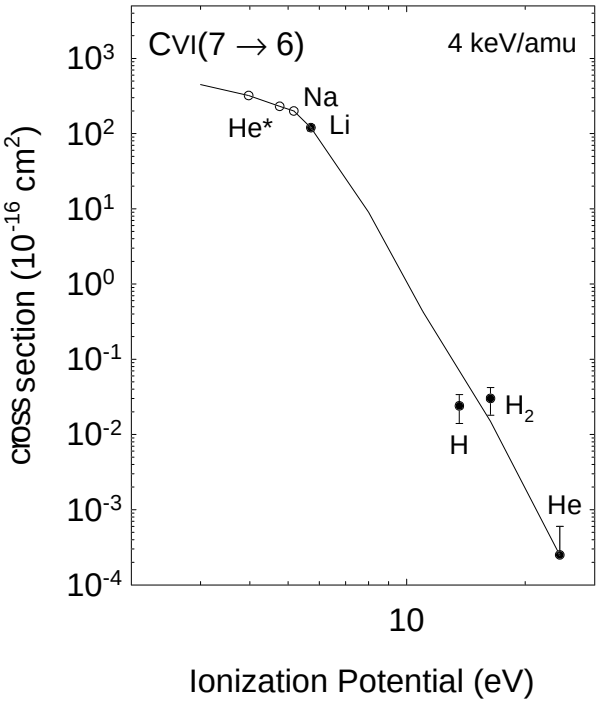

Figure 10 Summary of CIV($n = 7 \rightarrow n = 6$) line emission cross sections resulting from 4 keV/amu C6+ ions colliding on helium [129], atom [79] and molecular hydrogen [67], lithium [82], sodium [135], and metastable helium [129]. The latter result is based on CTMC calculations by Olson.

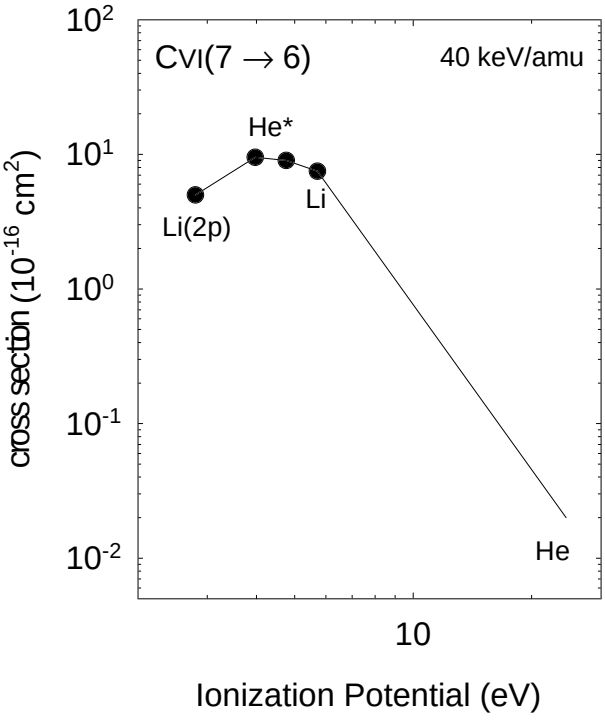

Figure 11 Summary of CIV($n = 7 \rightarrow n = 6$) line emission cross sections resulting from 40 keV/amu C^{6+} ions colliding on helium [129], lithium [82], and metastable helium [129]. The latter result is based on CTMC calculations by Olson.

The most promising concepts for power and particle control rely on atomic processes to transfer power and momentum from the edge plasma into the detached divertor plasma. The challenge is to develop a divertor design where atomic processes are sufficiently efficient to reduce the energy flux on the divertor plates by at least a factor of 5 to 10 (ITER requirement heatload: max. 5 MW/m^2). The radiation loss of impurities strongly increases with increasing Z and increasing electron density. The impurity density in the bulk plasma should be kept below the fraction below which ignition becomes impossible (e.g. 0.25% for iron, 2.4% for neon and 6.7% for carbon) while maximizing the impurity radiation in the divertor regime.

One of the key questions for the understanding of impurity dynamics in divertor plasmas is: what species are the main contributors to the total radiated power? This question can only be answered by means of spectroscopic studies. CXS offers not only a possibility to measure the temperature and density of the ionic species present in the divertor but it also offers an excellent possibility to track the sources of impurities in the divertor since the impurities that are released are generally ionized within 2-3 mm behind the point from where they are released. Therefore they can directly be associated with the surface from which they are released and thus CXS provides information on impurity sources, influx, sputtering yields, etc. On the other hand one should be aware of the fact that e^- collisions are competing with the charge exchange process. In view of recent studies by Maggi et al. electron impact excitation exceeds charge exchange under certain plasma conditions.

At JET a double SPRED VUV monochromator [139] is used for the observation of impurity spectra. This multichannel spectrometer allows simultaneous time resolved observation of transitions in the wavelength range between 10 and 170 nm. The materials that are presently used for the target plates in the divertor are beryllium and carbon, and therefore these are the main impurities in the divertor plasma. Moreover nitrogen, neon and argon are injected to enhance divertor cooling by radiation. Recent experiments at JET (pulse #34361 for example) where nitrogen was used as additional cooling gas show that approximately 80% of the total radiated power is emitted by nitrogen. Most of the power is emitted by NV and with decreasing intensities by NIV, NIII and NII.

Presently a full set of photon emissivity coefficients for nitrogen is not yet available in the ADAS data collection. The data set that is available for carbon is mainly based on theoretical data [109], [107] which are combined with total charge transfer measurements by Phaneuf et al. [88]. The state selective cross sections are benchmarked in the intermediate energy range by measurements by Hoekstra et al. [53] and at keV energies by measurements of Dijkkamp et al. [33]. The main difficulty that remains for the analysis of the CXS data on basis of these cross sections is the fact that there are still large discrepancies between the results of various theoretical models. In the relevant energy regime the data are at best

benchmarked by total charge transfer cross sections. This is not sufficient for reliable CXS modelling. Another difficulty that currently arises is the fact that JET is starting the full tritium phase. Now the plasma does not only contain deuterium but also tritium, which is used to initiate fusion reactions. The cross section data that are used for CXS modelling are based on charge exchange reactions with hydrogen but the first theoretical [121], [30] and experimental [114] investigations indicate that there are considerable differences between capture from the various isotopic species of hydrogen at low collision energies (see paragraph 2). Corresponding calculations have not yet been performed for carbon.

The experiments which are described in this thesis have been carried out to benchmark the theoretical models that are available in order to be able to establish a reliable data set which can be used as a basis for the ADAS calculations.